Carrier Phase Estimation in Multi-Subcarrier Coherent Optical Systems

Carrier Phase Estimation in Multi-Subcarrier Coherent Optical Systems

S. M. Bilal, Member, IEEE, C. Fludger, G. Bosco, Senior Member, IEEE

***Abstract*—In this letter we analyze three different carrier phase estimation approaches for coherent optical systems based on multi-subcarrier modulation, comparing them in terms of both performance and complexity. Averaging the estimated values on the subcarriers (SCs) significantly increases the laser linewidth tolerance at the expense of additional complexity, whilst using a single SC for carrier phase estimation yields a complexity reduction without any substantial performance loss with respect to performing a separate phase estimation on all SCs.**

***Index Terms*—Carrier phase estimation, Viterbi & Viterbi algorithm, quadrature amplitude modulation (QAM)**

I. Introduction

In the past few years, coherent optical detection has emerged as a compelling approach for optical communication systems. Coherent detection combined with digital signal processing (DSP) techniques can significantly increase the channel data rate, spectrum allocation and optical fiber communication capacity. Although linear impairments like polarization mode dispersion (PMD) and chromatic dispersion (CD) can be effectively compensated by DSP, performance of the optical communication system is still limited by the fiber non-linearities. In [1]–[3] it has been shown that the non-linear performance of coherent optical systems is significantly affected by the symbol rate: dividing the available bandwidth of a high baud-rate single-subcarrier (SC) into several low baud-rate subcarriers (SCs) can significantly improve the tolerance towards fiber non-linearities [4], [5]. For current 32 Gbaud systems, the optimum symbol rate for the SCs lies in the range of $2-4$ Gbaud and can result in $10\%-20\%$ increase in the maximum reach for polarization-multiplexed quadrature phase shift keying (PM-QPSK) systems [4], [5].

For multi-SC systems, phase noise resulting from the finite linewidth of transmitter laser (Tx) and receiver (Rx) local oscillator (LO) becomes more critical, since the symbol rate is reduced by a factor of N_{sc} where N_{sc} corresponds to the number of SCs for a multi-SC system. Let's assume that for a single-SC system the carrier phase estimation (CPE) scheme is able to tolerate a line-width times symbol duration product equal to $\Delta\nu \cdot T_s = \Delta\nu/R_s$, where R_s is the symbol rate ($R_s = 1/T_s$) and $\Delta\nu$ is the combined linewidth of Tx laser and LO. For a multi-SC system this tolerance decreases by $\Delta\nu/(R_s/N_{sc})$. As an example, if a particular CPE algorithm is characterized by $\Delta\nu/R_s = 6.25 \times 10^{-6}$, the combined linewidth tolerated by this algorithm in a 32-Gbaud SC system is 200 kHz ($\Delta\nu = (6.25\times10^{-6})\cdot(32\times10^{9})$). For a 4-SC and 8-SC systems this tolerance decreases to 50 kHz ($R_s = 32/4$ Gbaud) and 25 kHz ($R_s = 32/8$ Gbaud), respectively. As a consequence, while designing or implementing CPE algorithms for multi-SC systems special consideration should be taken.

This work was supported by CISCO Systems under an SRA Contract.

S. M. Bilal and G. Bosco are with Dipartimento di Elettronica, Politecnico di Torino, Italy (e-mail: bilalsyedm@gmail.com).

C. Fludger is with Cisco Optical GmbH, Nürnberg 90402, Germany (e-mail: cfludger@cisco.com).

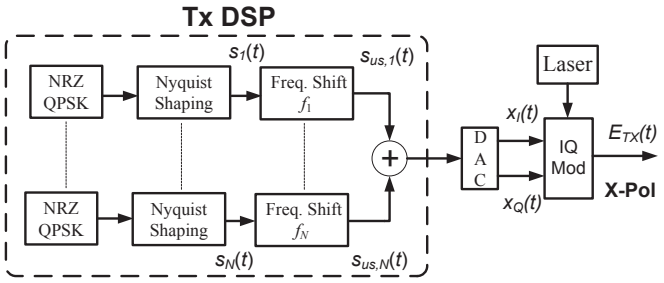

Fig. 1. Multi sub-carrier Tx schematics for polarization X. The same architecture is used to generate the signal for polarization Y.

In this paper we report an analysis of a Viterbi and Viterbi (V&V) Mth-Power feed forward CPE algorithm [6] for a multi-SC (8-SCs) PM-QPSK system using three different schemes:

- CPE1: CPE from a single SC applied to all SCs (low tolerance, low complexity)
- CPE2: CPE from individual SCs applied individually to all SCs (low tolerance, high complexity)
- CPE3: Average CPE from all SCs applied to all SCs (high tolerance, high complexity)

For the rest of the paper we would refer to CPE1, CPE2 and CPE3 as described above.

II. Multi-SC Simulation Setup

The Tx signal is composed of $\mathbf{N_{sc}} = \mathbf{8}$ SCs based on quadrature-phase shift-keying (QPSK) modulation [7]. They are generated in the digital domain, as shown in Fig. 1. A set of baseband signals $s_n(t)$, with $\mathbf{n} = \mathbf{1}, \ldots, \mathbf{N_{sc}}$, each of symbol rate R_{SC}, is created. Each baseband signal is Nyquist filtered in order to obtain pulses with a square root raised cosine (SRRC) Fourier transform, with roll-off 0.05. The signals $s_n(t)$ are then digitally up-shifted to their respective center frequency:

$$f_n = \left(n - \frac{(N_{sc}+1)}{2}\right) \cdot \Delta f \tag{1}$$

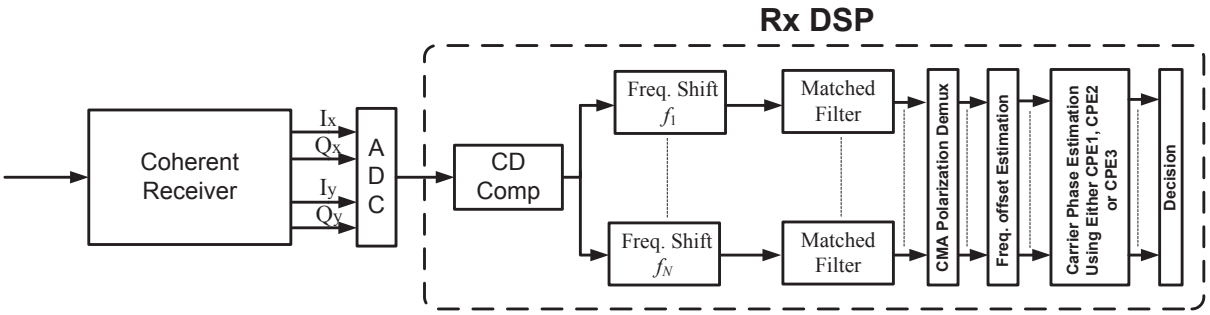

Fig. 2. Multi subcarrier Rx schematics. Carrier phase estimation is performed either using the algorithms CPE1, CPE2 or CPE3 described in Fig. 3.

$\Delta f = 1.05 \cdot R_{SC}$ is the spacing between the SCs. Note that the aggregate channel symbol rate is equal to $R_s = \mathbf{N_{sc}} \cdot \mathbf{R_{SC}}$. The SCs are multiplexed and their samples fed to a digital-to-analog converter (DAC), which generates the electrical signals $x_I(t)$ and $x_Q(t)$, corresponding to the in-phase and quadrature components of the transmitted electrical signal. The two components are then input to a standard IQ modulator. The complex envelope of the optical transmitted signal for a single polarization can then be written as:

$$E_{Tx}(t) = \sum_{n=1}^{N_{sc}} s_n(t) e^{j2\pi f_n t} \tag{2}$$

The signal at the output of the transmitter is finally polarization-multiplexed with a similar signal generated for the Y polarization, forming a complete channel which could then be wavelength-multiplexed with others and transmitted through an optical link. The Rx (see Fig. 2) is a standard polarization-diversity coherent receiver with an analog-to-digital converter (ADC) which samples the incoming signals at a speed equal to $2 \cdot R_s$. DSP blocks follow, including a static filter for chromatic dispersion (CD) compensation, frequency down-shift to translate to baseband all SCs for demodulation, a static matched filter with square-root raised-cosine (SRRC) transfer function, constant modulus algorithm (CMA) for polarization demultiplexing, frequency offset compensation, carrier phase estimation using either CPE1, CPE2 or CPE3 algorithms and finally a decision block for calculating bit-error-rate (BER). In our simulations, the same 45-taps butterfly equalizer was used for all SCs, in order to avoid the random phase rotations among the different SCs. The equalizer taps were updated using a CMA, with the error evaluated processing one of the two center SCs.

In our simulations we have modeled laser phase noise as a Wiener process [8]:

$$\theta_k = \sum_{i=-\infty}^{k} v_i \tag{3}$$

θ_k is the laser phase noise and v_i's are independent and identically distributed Gaussian random variables with zero mean and variance

$$\sigma_f^2 = 2\pi\Delta\nu \cdot T_s \tag{4}$$

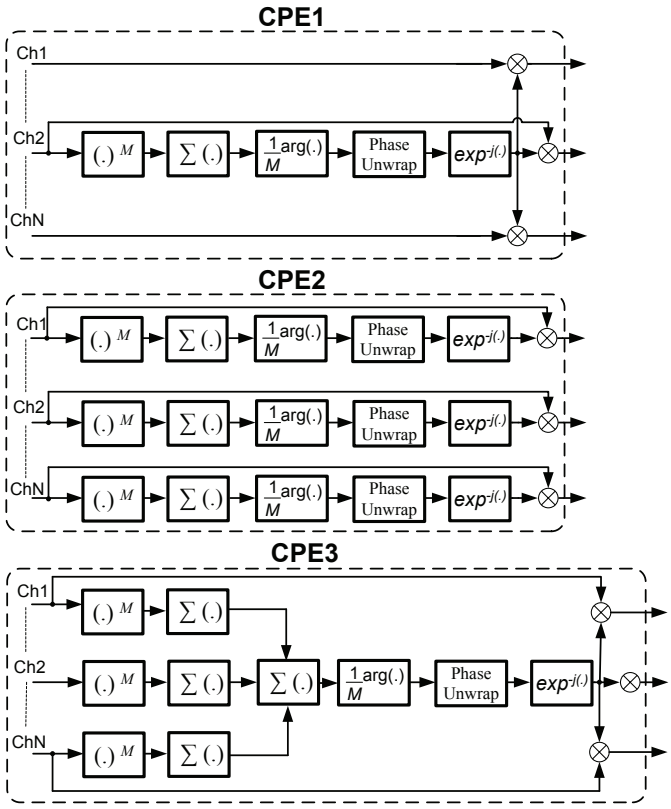

Fig. 3. Schematic digram for all the three cases. CPE1 makes the estimate from any of the SCs and apply it to all the SCs. CPE2 makes the estimate from individual SCs and apply it individually on all the SCs. CPE3 makes an average estimate from all the SCs and apply it to all the SCs.

$\Delta\nu$ is the laser linewidth and $\mathbf{T_s} = \mathbf{1}/\mathbf{R_s}$ is the symbol period.

V&V algorithm is used for CPE either using CPE1, CPE2 or CPE3 algorithms. The schematic diagram for all the three cases is shown in Fig. 3. CPE1 estimates the phase error by using the data from a single SC and applies it to all the SCs. For our setup we observed that the performance is independent of the SC used for phase estimation. CPE2 estimates the phase errors on each SC and applies them individually on all the SCs. CPE3 makes an average estimate from all the SCs and applies it to all the SCs. **For CPE3, averaging of all the SCs is done using a summation block instead of an averaging block. This is because a real-number divider for averaging does not affects the phase calculations**.

Although this preliminary study is focused on back-to-back performance, it is important to note that in a real system, after fiber propagation, there will be a constant phase offset between different SCs. In order to correct that offset a training sequence can be used to calculate the delay (in terms of number of symbols) between the transmitted and received data and the estimated delay can further be used to correct the phase offset between different SCs after down conversion. Consider for instance the case of a single-SC system. The transmitted data samples $x(t)$ digitally up-shifted to their center frequency f_i can be written as:

$$x(t)e^{j2\pi f_i t} \tag{5}$$

After propagating through the fiber, Eq. (5) will become

$$x(t+\tau)e^{j2\pi f_i(t+\tau)} \tag{6}$$

where τ is the propagation delay. After down-shifting at the receiver side, Eq. (6) becomes

$$x(t+\tau)e^{j2\pi f_i(t+\tau)}e^{-j2\pi f_i(t)} = x(t+\tau)e^{j\phi} \tag{7}$$

where the constant $\phi = 2\pi f_i(\tau)$ results in phase rotation, proportional to the propagation delay τ.

III. Simulation Results

Fig. 4 shows the performance comparison of all the three algorithms using the conventional V&V scheme. The values of N reported in the legend indicate the lengths of averaging windows, optimized by maximizing the linewidth tolerance at 1-dB penalty [9]. Curves obtained with and without differential encoding (DE) are shown in Fig. 4. Angle differential encoding [10] is used to avoid cycle slips that could occur at high $\Delta\nu{\cdot}T_s$ values. For this reason, the curves without DE cannot go higher because of the cycle slips that could occur at high $\Delta\nu \cdot T_s$, indicating that without DE, a pilot-symbol/tone based recovery is needed and hence a pilot-based cycle slip recovery method would be required.

Fig. 5 shows the required signal-to-noise-ratio (SNR) vs Window Length (N) to achieve a BER=10^{-2}. Fig. 6 gives optimum window length (N) and the corresponding SNR at that window length for different $\Delta\nu \cdot T_s$ values at BER=10^{-2}. Higher the value of $\Delta\nu \cdot T_s$ higher will be the SNR and lower will be N. A larger value of N is needed for amplified spontaneous emission (ASE) noise whereas on the other hand a smaller value of N is required for a better CPE. Large and small values of N correspond to large and small averaging window lengths for V&V. A large averaging window will properly counter ASE noise whereas smaller averaging window lengths are critical for phase noise compensation. So the value of N is based on a compromise between ASE noise and phase noise. In our simulations we have chosen it from Fig. 5 and Fig. 6 by maximizing the linewidth tolerance at 1-dB penalty. Curves in Fig. 5 and 6 referred to differentially encoded data. The reference SNR without phase noise and CPE for differentially encoded data was found to be 8.1 dB at BER=10^{-2}.

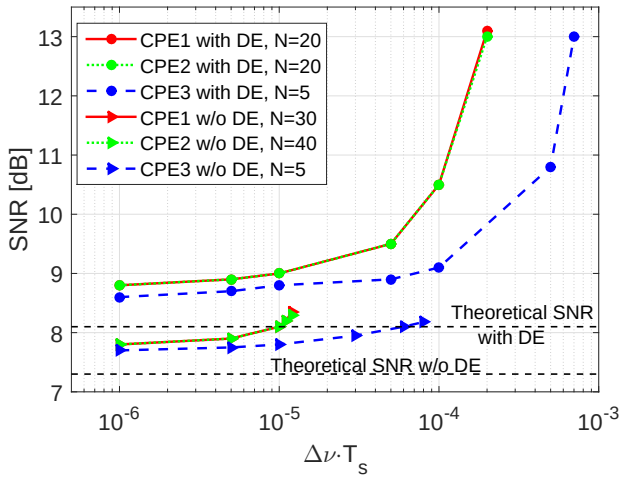

Fig. 4. SNR vs linewidth times symbol duration ($\Delta\nu \cdot T_s$) product at BER=10^{-2} for all the three cases. DE refers to differential encoding.

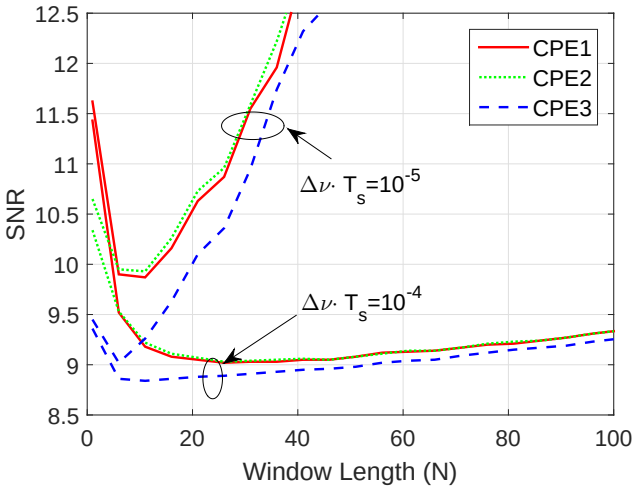

Fig. 5. SNR vs window length (N) at BER=10^{-2} for different $\Delta\nu \cdot T_s$ values. For simplicity only two $\Delta\nu \cdot T_s$ values are shown.

Assuming a receiver sensitivity penalty of 1-dB at a target BER=10^{-2}, the tolerance of CPE1 and CPE2 is $\approx 1.2 \times 10^{-5}$ whereas the tolerance of CPE3 is $\approx 1.0 \times 10^{-4}$. For our simulations we have chosen the target BER=10^{-2} so that the system can tolerate a 1-dB SNR penalty due to phase noise without exceeding the FEC threshold, which is assumed to be 2×10^{-2}, as granted by current state-of-the-art soft FEC codes with 20% overhead [11].

Table I [9] shows the complexity comparison of all the three cases. Although the performance of CPE2 is the same as that of CPE1, its complexity is almost N_{sc} times more than that of CPE1. CPE3 has almost the same complexity as that of CPE2 but performance is much better than either CPE1 or CPE2. The complexity evaluations reported in Table I are referred to the processing of a single polarization with phase unwrapping and optimum implementation [9]. For example, by doing some mathematical computations it can be shown that the 4^{th} power of a complex value needs only 6 real multipliers and 2 adders

TABLE I
COMPUTATIONAL COMPLEXITY FOR THE THREE CASES.

Algorithm	Real Multipliers	Real Adders	Comparators	Look-Up Tables	Decisions
CPE1	$8N$	$3N+2$	0	1	N
CPE2	$N_{sc} \times 8N$	$N_{sc}(3N+2)$	0	1	$N_{sc} \times N$
CPE3	$N_{sc} \times 8N$	$N_{sc}(3N+2)+2(N_{sc}-1)$	0	1	$N_{sc} \times N$

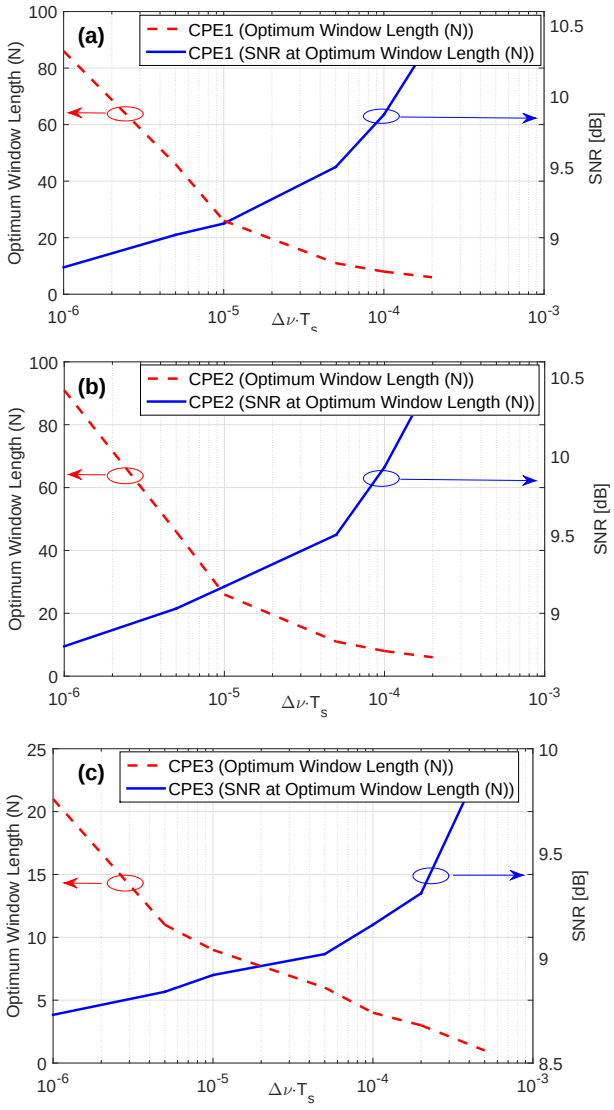

Fig. 6. Optimum window length and the corresponding SNR at that window length (N) vs $\Delta\nu \cdot T_s$ at BER=10^{-2}. (a), (b) and (c) are for CPE1, CPE2 & CPE3 respectively. Red dashed curves in (a), (b) and (c) are for optimum window length, whereas blue curves correspond to SNR at that window length.

instead of 8 real multipliers and 4 adders. The complexity computations however do not consider the normalization factor and phase derotations.

IV. CONCLUSION

In this paper, we have analyzed through simulations three different carrier phase estimation schemes using V&V algorithm for a multi-SC optical communication system. CPE1 (i.e CPE from a single SC applied to all SCs) and CPE2 (i.e CPE from individual SCs applied individually to all SCs) can tolerate a $\Delta\nu \cdot T_s \approx 1.2 \times 10^{-5}$ at 1-dB SNR penalty, but the complexity of CPE2 is almost N_{sc} times higher than that of CPE1. The tolerance of CPE3 (average CPE from all SCs applied to all SCs) is much higher than either of CPE1 or CPE2 with $\Delta\nu \cdot T_s \approx 1.0 \times 10^{-4}$ at 1-dB SNR penalty but with complexity almost the same as CPE2 and higher than CPE1. In general, averaging the carrier phase estimation over $\mathbf{N_{sc}}$ SCs gives a proportional improvement in performance. So a compromise has to be made between the complexity and performance while evaluating the carrier phase for these multi-SC optical communication systems.

REFERENCES

[1] L. B. Du and A. J. Lowery, "Optimizing the subcarrier granularity of coherent optical communications systems," *Opt. Express*, vol. 19, no. 9, pp. 8079–8084, Apr 2011. [Online]. Available: http://www.opticsexpress.org/abstract.cfm?URI=oe-19-9-8079

[2] W. Shieh and Y. Tang, "Ultrahigh-speed signal transmission over nonlinear and dispersive fiber optic channel: The multicarrier advantage," *Photonics Journal, IEEE*, vol. 2, no. 3, pp. 276–283, June 2010.

[3] A. Bononi, N. Rossi, and P. Serena, "Performance dependence on channel baud-rate of coherent single-carrier WDM systems," in *Proc. of ECOC 2013, London (United Kingdom), paper Th.1.D.5*, September 2013.

[4] M. Qiu, Q. Zhuge, X. Xu, M. Chagnon, M. Morsy-Osman, and D. Plant, "Subcarrier multiplexing using dacs for fiber nonlinearity mitigation in coherent optical communication systems," in *Proc. of OFC/NFOEC 2014, San Francisco, paper Tu3J.2*, March 2014.

[5] A. Nespola, L. Bertignono, G. Bosco, A. Carena, Y. Jiang, S. M. Bilal, P. Poggiolini, S. Abrate, and F. Forghieri, "Experimental demonstration of fiber nonlinearity mitigation in a WDM multi-subcarrier coherent optical system," in *Proc. of ECOC 2015, Valencia (Spain), paper Mo.3.6.3*, September 2015.

[6] A. Viterbi, "Nonlinear estimation of PSK-modulated carrier phase with application to burst digital transmission," *Information Theory, IEEE Transactions on*, vol. 29, no. 4, pp. 543–551, 1983.

[7] G. Bosco, S. M. Bilal, A. Nespola, P. Poggiolini, and F. Forghieri, "Impact of the transmitter IQ-skew in multi-subcarrier coherent optical systems," in *Proc. of OFC/NFOEC 2016, Anaheim, paper W4A.5*, March 2016.

[8] S. M. Bilal, C. Fludger, V. Curri, and G. Bosco., "Multi-stage CPE algorithms for phase noise mitigation in 64-QAM optical systems," *J. Lightwave Technol.*, vol. 32, no. 17, pp. 2973–2980, September 2014.

[9] S. M. Bilal, G. Bosco, J. Cheng, A. P. T. Lau, and C. Lu, "Carrier phase estimation through the rotation algorithm for 64-QAM optical systems," *J. Lightwave Technol.*, vol. 33, no. 9, pp. 1766–1773, May 2015.

[10] J.-K. Hwang, Y.-L. Chiu, and C.-S. Liao, "Angle differential-QAM scheme for resolving phase ambiguity in continuous transmission system," *Int. J. Commun. Syst.*, vol. 21, no. 6, pp. 631–641, 2008.

[11] Y. Miyata, K. Sugihara, W. Matsumoto, K. Onohara, T. Sugihara, K. Kubo, H. Yoshida, and T. Mizuochi, "A triple-concatenated FEC using soft-decision decoding for 100 Gb/s optical transmission," in *Proc. of OFC/NFOEC 2010, San Diego, paper OThL3*, March 2010.